Organic LETTERS

Letter

pubs.acs.org/OrgLett

Theoretical Study of Nickel-Catalyzed Proximal C−C Cleavage in Benzocyclobutenones with Insertion of 1,3-Diene: Origin of Selectivity and Role of Ligand

Shengwen Yang, Yilu Xu, and Juan Li*

Department of Chemistry, Jinan University, Huangpu Road West 601, Guangzhou, Guangdong 510632, P. R. China

Supporting Information

ABSTRACT: Martin and co-workers recently developed a strategy for Ni(0)-complex-catalyzed [4 + 4] annulation of primary benzocyclobutenones (BCBs) and 1,3-dienes. A density functional theory study was performed to clarify the catalytic mechanism. The results provide insights into the origins of the chemo-, regio-, and diastereoselectivity. The calculation results explain why only $P(C_6H_5CF_3)_3$, among several candidates, performed well and why the [4 + 4] annulation of BCB with a 1,3-diene was achieved with a Ni(0) but not with a Rh(I) catalyst.

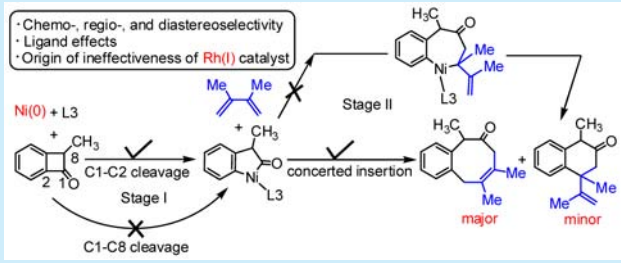

Transition-metal-catalyzed C−C bond activation with subsequent functionalization has great potential in the synthesis of complex product scaffolds.[1] Although of significant interest, catalytic C−C activation has been much less explored than the related C−H activation because cleavage of the strong C−C bond is hampered by the increased steric congestion at the C−C bond relative to that at the C−H bond.[2] The transition-metal-catalyzed ring-opening reactions of highly strained three- or four-membered rings are a central theme in C−C bond activation strategies.[3,4] Benzocyclobutenones (BCBs) have been used in reactions involving the activation and subsequent functionalization of C−C bonds.[5] Cleavage of the C−C bond in a BCB followed by π-component insertion has been achieved using transition metals. However, the scope of the unsaturated π-component has been mainly restricted to alkenes and alkynes. The intermolecular insertion of 1,3-dienes has rarely been explored.

Recently, Martin's group reported room-temperature Ni-catalyzed intermolecular proximal C1−C2 cleavage in BCBs with 1,3-diene insertion (Scheme 1).[6] This is the first report of metal-catalyzed proximal C1−C2 cleavage in a BCB without prior carbonyl activation or the use of noble metals. One of the key aspects of the results reported by Martin et al. is the intriguing chemo-, regio-, and diastereoselectivity profile. Experiments showed that the reactivity of the Ni catalyst in the [4 + 4] annulation reaction is greatly affected by the ligand. Importantly, this intermolecular [4 + 4] annulation of a BCB with 1,3-diene insertion cannot be achieved using Rh(I) catalysts, although these are common catalysts for C−C bond cleavage in BCBs.[5] We performed a density functional theory (DFT) mechanistic study to gain insights into this strategy based on structures and energetics that are often difficult to access experimentally. The results should enable the strategy to be more widely used.

Scheme 1. Ni-Catalyzed Intermolecular [4 + 4] Annulation of BCB with Insertion of 1,3-Diene Reported by Martin's Group

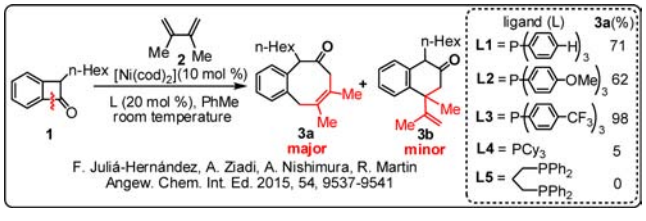

All calculations were performed at the B3LYP theoretical level using the Gaussian 09 package.[7] We chose **L3** in Scheme 1 as the ligand for our mechanistic investigation because it was the most effective ligand experimentally. In the calculations, a methyl group was used instead of *n*-hexyl as the substituent in the BCB to reduce the computational costs.[8] The catalytic [4 + 4] annulation of a BCB with insertion of a 1,3-diene proceeds via two stages; stage I involves C−C bond cleavage, and stage II involves 1,3-diene insertion.

The energy profiles for C−C bond cleavage (stage I) are shown in Figure 1 (black line for C1−C2 bond cleavage and red line for C1−C8 bond cleavage). The first step involves coordination of $\mathbf{1}_{Me}$ to $Ni(L3)_2$. In the route shown by the black line in Figure 1, BCB ring opening through C1−C2 single-bond cleavage takes place to give **A** by spanning a barrier of 23.9 kcal/mol ($\mathbf{TS}_{A1\text{-}A}$). The subsequent release of **L3** leads to formation of the stable 14e Ni(II) complex **D** (−27.8 kcal/mol), which is further transformed to **E** through coordination of **2** to Ni. For the red line in Figure 1, C1−C8 single-bond cleavage gives **B**, with an energy barrier of 28.8 kcal/mol. The five-

Received: September 29, 2016
Published: December 5, 2016

DOI: 10.1021/acs.orglett.6b02943
Org. Lett. 2016, 18, 6244−6247

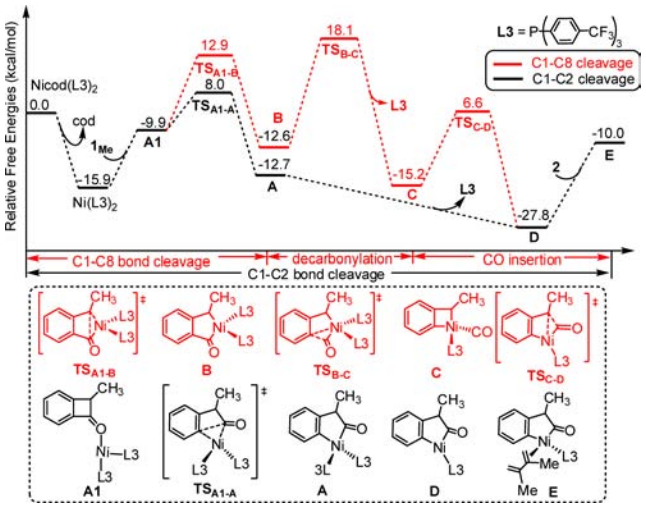

Figure 1. Energy profiles calculated for stage I. $\mathbf{1}_{Me}$ → **E** (black line for C1−C2 cleavage and red line for C1−C8 cleavage). Solvent-corrected free energies are given in kcal/mol.

membered nickelacycle **B** is transformed to the four-membered nickelacycle **C** through decarbonylation; this has a high energy barrier of 34.0 kcal/mol relative to Ni(**L3**)$_2$ + $\mathbf{1}_{Me}$. CO then inserts into the Ni−C8 bond via transition state $\mathbf{TS}_{C\text{-}D}$, generating **D**. Intermediate **D** coordinates to **2** to give the 16e Ni(II) complex **E**. The energy barrier for the C1−C8 cleavage process is 34.0 kcal/mol, which is 10.1 kcal/mol higher than that for C1−C2 cleavage.

Previous DFT calculations performed by Liu et al.[9] showed that C1−C8 cleavage was more favorable than C1−C2 cleavage when Rh(I) was used as the catalyst. We speculated that the steric hindrance caused by the methyl group at C8 of BCB is the origin of preferential C1−C2 cleavage over C1−C8 cleavage. We investigated this by replacing the methyl group in $\mathbf{1}_{Me}$ with a hydrogen atom and computed the C1−C2 and C1−C8 cleavage steps (Scheme S2). Although the difference (4.0 kcal/mol) between the free-energy barriers for C1−C2 and C1−C8 cleavage is smaller in the case of hydrogen, C1−C8 cleavage cannot override C1−C2 cleavage. Next, we evaluated the two C−C bond cleavage modes (Scheme S2) for a C3-substituted BCB, which is the substrate used in the calculations by Liu et al.[9] The calculations show that, for a C3-substituted BCB, the barrier for C1−C8 cleavage (26.0 kcal/mol) is slightly higher than that for C1−C2 cleavage (25.2 kcal/mol). Steric hindrance at the C3 position of BCB therefore cooperates with the Rh(I) catalyst[10] to make C1−C8 cleavage more favorable than C1−C2 cleavage, as reported by Liu.

After C−C bond cleavage, 1,3-diene insertion from intermediate **E** occurs (stage II). In stage II, four possible pathways (paths a−d) are considered for 1,3-diene insertion. In path a, the 1,3-diene inserts into the Ni−C1 bond in a concerted fashion via $\mathbf{TS}_{E\text{-}H}$ to form **H**, with a barrier of 13.9 kcal/mol relative to **E**. As shown in Figure 2, $\mathbf{TS}_{E\text{-}H}$ is a six-membered transition state with the two terminal carbon atoms in the 1,3-diene molecule inserted into the Ni−C1 bond. **H** then undergoes reductive elimination via transition state $\mathbf{TS}_{H}$ to generate the product $\mathbf{3a}_{Me}$, with regeneration of the catalyst Ni(**L3**)$_2$. $\mathbf{TS}_{H}$ has an activation energy barrier of 19.5 kcal/mol with respect to **H**. In path b (blue line in Figure 2), a nine-membered nickelacycle **I** is formed through concerted 1,3-diene insertion into the Ni−C2 bond via transition state $\mathbf{TS}_{E\text{-}I}$, overcoming a barrier of 18.2 kcal/

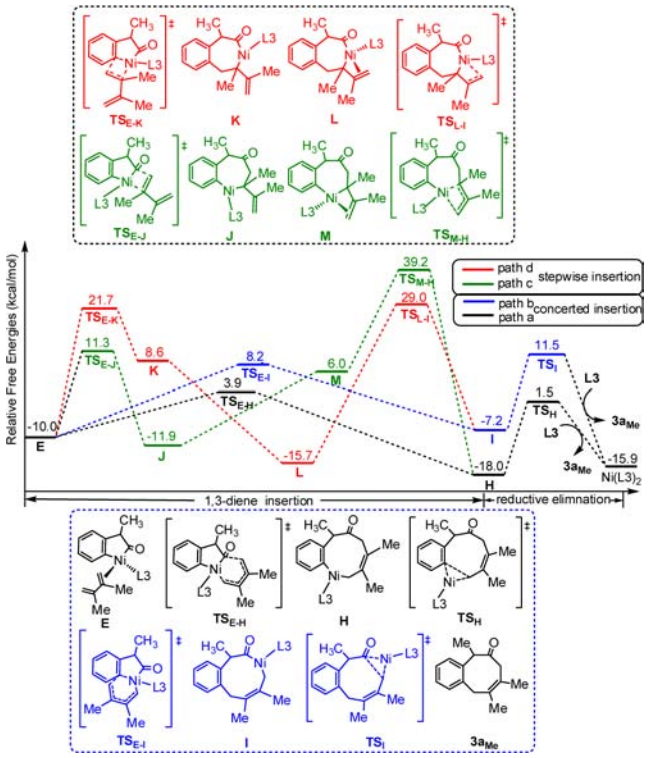

Figure 2. Energy profiles calculated for stage II. **E** → $\mathbf{3a}_{Me}$ (paths a−d). Solvent-corrected free energies are given in kcal/mol.

mol relative to **E**. Subsequent C−C-bond-forming reductive elimination via $\mathbf{TS}_{I}$ generates the [4 + 4] product $\mathbf{3a}_{Me}$ and regenerates the catalyst, overcoming a barrier of 18.7 kcal/mol relative to **I**.

The free energy of $\mathbf{TS}_{E\text{-}I}$ is higher than that of $\mathbf{TS}_{E\text{-}H}$, which indicates that 1,3-diene insertion into the Ni−C1 bond is more favorable than insertion into the Ni−C2 bond. To gain insights into the difference between these two insertion modes, transition states $\mathbf{TS}_{E\text{-}H}$ and $\mathbf{TS}_{E\text{-}I}$ were examined using distortion/interaction analysis (Figure 3).[11,12] This method involves

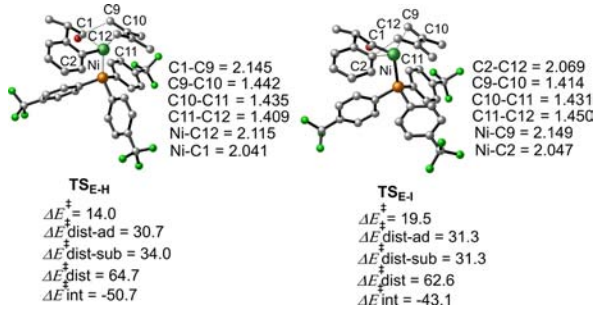

Figure 3. Optimized structures of transition states $\mathbf{TS}_{E\text{-}H}$ and $\mathbf{TS}_{E\text{-}I}$, along with key bond lengths (in angstroms). Hydrogen atoms are omitted for clarity. Distortion/interaction energies are given in kcal/mol.

splitting the activation energy ($\Delta E^{\ddagger}_{dist}$) into a steric component (distortion energy $\Delta E^{\ddagger}_{dist}$) and an electronic component (interaction energy $\Delta E^{\ddagger}_{int}$). The total distortion energy of $\mathbf{TS}_{E\text{-}H}$ is 2.1 kcal/mol higher than that of $\mathbf{TS}_{E\text{-}I}$. However, the interaction energy of $\mathbf{TS}_{E\text{-}H}$ (−50.7 kcal/mol) is significantly more negative than that of $\mathbf{TS}_{E\text{-}I}$ (−43.1 kcal/mol), suggesting

DOI: 10.1021/acs.orglett.6b02943
Org. Lett. 2016, 18, 6244−6247

Table 1. Effects of Ligand on Activation Barrier[a]

ligand	3a (%)	A1(L)	TS_{A1-A}(L)	A(L)	D(L)	E(L)	TS_{E-J}(L)	TS_{E-H}(L)
L1	71	−9.0	6.4	−14.7	−29.7	−12.3	8.8	2.6
L2	62	−8.4	5.5	−15.3	−31.3	−13.2	7.1	1.8
L3	98	−9.9	8.0	−12.7	−27.8	−10.0	11.3	3.9
L4	5	−10.6	25.2	−9.4	−29.4	−9.2	17.4	12.1
L5	0	2.9	13.1	−8.9	−3.3	12.0	35.0	27.7

[a]Free energies are relative to $\mathbf{1}_{Me}$ + $Ni(L)_2$ and given in kcal/mol.

that the significant interaction energy difference between TS_{E-H} and TS_{E-I} is important.

In path c, the two double bonds of the 1,3-diene are sequentially inserted into the Ni−C1 bond via TS_{E-J} and TS_{M-H}, respectively, with relative free energies of 11.3 and 39.2 kcal/mol, respectively (Figure 2). Path d also involves stepwise insertion via TS_{E-K} and TS_{L-I}, respectively, with relative free energies of 21.7 and 29.0 kcal/mol. Insertion of the first double bond of the 1,3-diene is clearly more favorable than that of the second double bond in paths c and d. As indicated in Figure 2, one-step concerted insertions (paths a and b), which have barriers of 31.7 and 36.0 kcal/mol, are much more favorable than the two-step processes (paths c and d), with rate-determining barriers of 67.0 and 56.8 kcal/mol, respectively. Importantly, transition states TS_{E-H} (concerted mechanism) and TS_{E-J} (stepwise mechanism) are responsible for formation of the products $\mathbf{3a}_{Me}$ and $\mathbf{3b}_{Me}$, respectively (i.e., chemoselectivity for [4 + 4] over [4 + 2] annulation).[13] The preference for $\mathbf{3a}_{Me}$ can be attributed to the distortion energy of the four-membered ring in TS_{E-J} being larger than that in the six-membered ring in TS_{E-H}.

We investigated the origins of the effects of the phosphine ligand on the reactivity and chemoselectivity by computing the key intermediates and transition states for the other ligands shown in Scheme 1. Good agreement with the trends in the experimental reactivity and chemoselectivity was obtained (Table 1).[14] The barrier for 1,3-diene insertion for the electron-rich triarylphosphine **L2** (33.1 kcal/mol) is higher than that for **L3** (31.9 kcal/mol) for the following reasons (Scheme 2). Connection of the electron-donating ligand **L2** to

Scheme 2. Explanation for Ligand Effect

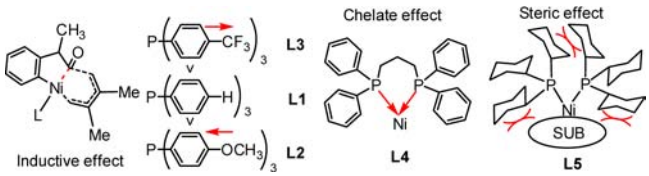

Ni strengthens the Ni−C1 bond against 1,3-diene insertion. The experimentally ineffective **L4** ligand has a barrier of 46.8 kcal/mol for the 1,3-diene insertion step. **L4** is a bulky ligand, and the steric repulsion in the transition state $TS(L4)_{E-H}$, shown by the shortest nonbonding H···H distance of 2.07 Å between the **L4** ligand and 1,3-diene, results in low reactivity. For the bidentate ligand **L5**, dissociation of one arm (−PPh_2) from the Ni center to form **D(L5)** is necessary to provide a vacant coordination site at the Ni center, which enables coordination of the 1,3-diene substrate. The process from **A(L5)** to **E(L5)** is endergonic by 20.9 kcal/mol. The energy barrier for 1,3-diene insertion from **E(L5)** via $TS(L5)_{E-H}$ is 23.0 kcal/mol. Dissociation of **L5** to give the disfavored monodentate coordination mode is therefore highly endergonic, which increases the energy barrier of the 1,3-diene insertion step.[15]

We chose the standard experimental compound 1-phenyl-1,3-butadiene as a representative system and computed the regio- and diastereoselectivity of the reaction. The regio- and diastereoselectivity originate in the 1,3-diene insertion step. Our calculations indicate that the 1,3-diene insertion step for the *anti* product is more facile than that for the *syn* product ($^{syn}TS(2f)_{E-H}$ in Scheme 3: 0.2 kcal/mol vs $^{anti}TS(2f)_{E-H}$ in

Scheme 3. Calculated Regio- and Diastereoselectivity[a]

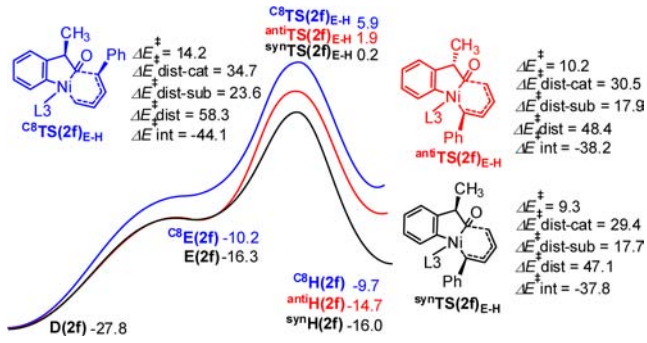

[a]Distortion/interaction energies are given in kcal/mol.

Scheme 3: 1.9 kcal/mol).[16] The 1,3-diene insertion step for the C5-product is also easier than that for the C8-product ($^{syn}TS(2f)_{E-H}$ in Scheme 3: 0.2 kcal/mol vs $^{C8}TS(2f)_{E-H}$ in Scheme 3: 5.9 kcal/mol). The reason for these results was clarified based on a distortion/interaction model; the regio- and diastereoselectivity are mainly controlled by the distortion energy.

Next, we explain why the [4 + 4] annulation of a BCB with a 1,3-diene does not occur with commonly used Rh(I) catalysts.[6] We considered two Rh(I) catalysts, i.e., RhCl(dppb) [dppb = 1,4-bis(diphenylphosphino)butane] and Rh(OH)(COD) (COD = cycloocta-1,5-diene), which have previously been reported to be active catalysts.[5] The detailed results are shown in Scheme 4. The calculated energy barriers for C1−C2 cleavage in the RhCl(dppb) and Rh(OH) (COD) systems (31.3 and 27.1 kcal/mol, respectively) are much higher than that for the Ni(0) system (23.9 kcal/mol); this is consistent with the experimental observations.[6] We propose that the difference can be explained by control of the reactivity by a trans effect in the transition state in C1−C2 cleavage. C1−C2 cleavage generates acyl and phenyl ligands, which have strong trans effects. In $^{RhCl}TS_{A1-A}$ and $^{Rh(OH)}TS_{A1-A}$, the phosphine ligand has to be *trans* to the phenyl ligand, and this is not favored because of the trans effect. In contrast, TS_{A1-A} adopts a four-coordinated tetrahedral structure, which avoids the trans effect. The lower barrier for $^{Rh(OH)}TS_{A1-A}$ than for $^{RhCl}TS_{A1-A}$ can be attributed to the trans effect between phenyl and COD being less strong than that between phenyl and

DOI: 10.1021/acs.orglett.6b02943
Org. Lett. 2016, 18, 6244−6247

Scheme 4. C1−C2 Cleavage in RhCl(dppb) and Rh(OH)(COD) Systems[a]

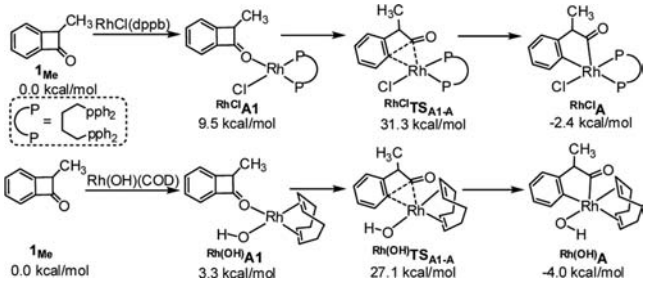

[a]All of the values are solvent-corrected free energies in kcal/mol.

phosphine. Furthermore, the overall barriers in the RhCl(dppb) and Rh(OH)(COD) systems (47.4 and 33.2 kcal/mol in Scheme S6, respectively) are also higher than that in the Ni(0) system (31.7 kcal/mol).

A novel synthetic strategy based on [4 + 4] annulation of a primary benzocyclobutenone and 1,3-diene without prior carbonyl activation or the use of noble metals was recently developed by Martin et al. We performed a DFT study to clarify the catalytic mechanism of the system. The origin of the chemoselectivity for [4 + 4] annulation over [4 + 2] annulation was investigated; [4 + 2] annulation is unfavorable because of the large distortion energy of the four-membered ring in the transition state in stepwise insertion. The regio- and diastereoselectivity for unsymmetrical 1,3-dienes are mainly controlled by the distortion energy. Our computational results successfully explain the experimentally observed result that only the monodentate triarylphosphine **L3**, among several candidates, performed well. The steric effect of **L4** and electronic effect of **L2** significantly affect the free-energy barrier, and this ultimately affects their reactivities. For the **L5** ligand, the 1,3-diene insertion step requires the energetically unfavorable partial dissociation of **L5**, which leads to a high barrier to the 1,3-diene insertion step. We suggest that Rh(I) catalysts are ineffective because of a strong trans effect.

■ ASSOCIATED CONTENT

Supporting Information

The Supporting Information is available free of charge on the ACS Publications website at DOI: 10.1021/acs.orglett.6b02943.

Computational details, calculated imaginary frequencies of all transition state species, additional computational results, table of calculated energies, and Cartesian coordinates of all calculated structures (PDF, XYZ)

■ AUTHOR INFORMATION

Corresponding Author

*E-mail: tchjli@jnu.edu.cn.

ORCID

Juan Li: 0000-0003-0693-3162

Notes

The authors declare no competing financial interest.

■ ACKNOWLEDGMENTS

This work was supported by the National Natural Science Foundation of China (Grant No. 21573095), the Fundamental Research Funds for the Central Universities (Grant No. 21615405), and the high-performance computing platform of Jinan University.

■ REFERENCES

(1) For selected reviews, see: (a) Seiser, T.; Cramer, N. *Org. Biomol. Chem.* **2009**, *7*, 2835−2840. (b) Rubin, M.; Rubina, M.; Gevorgyan, V. *Chem. Rev.* **2007**, *107*, 3117−3179. (c) van der Boom, M. E.; Milstein, D. *Chem. Rev.* **2003**, *103*, 1759−1792. (d) Ruhland, K. *Eur. J. Org. Chem.* **2012**, *2012*, 2683−2706. (e) Dermenci, A.; Coe, J. W.; Dong, G. *Org. Chem. Front.* **2014**, *1*, 567−581. (f) Souillart, L.; Cramer, N. *Chem. Rev.* **2015**, *115*, 9410−9464. (g) Chen, F.; Wang, T.; Jiao, N. *Chem. Rev.* **2014**, *114*, 8613−8661.

(2) (a) Rybtchinski, B.; Milstein, D. *Angew. Chem., Int. Ed.* **1999**, *38*, 870−883. (b) Corbet, J.-P.; Mignani, G. *Chem. Rev.* **2006**, *106*, 2651−2710.

(3) For selected reviews, see: (a) Winter, C.; Krause, N. *Angew. Chem., Int. Ed.* **2009**, *48*, 2460−2462. (b) Seiser, T.; Saget, T.; Tran, D. N.; Cramer, N. *Angew. Chem., Int. Ed.* **2011**, *50*, 7740−7752. (c) C−C Bond Activation. In *Topics in Current Chemistry*; Dong, G., Ed.; Springer-Verlag: Berlin, 2014; Vol. *346*.

(4) For some recent examples, see: (a) Ishida, N.; Ikemoto, W.; Murakami, M. *J. Am. Chem. Soc.* **2014**, *136*, 5912−5915. (b) Souillart, L.; Cramer, N. *Angew. Chem., Int. Ed.* **2014**, *53*, 9640−9644. (c) Ding, L.; Ishida, N.; Murakami, M.; Morokuma, K. *J. Am. Chem. Soc.* **2014**, *136*, 169−178. (d) Xia, Y.; Liu, Z.; Liu, Z.; Ge, R.; Ye, F.; Hossain, M.; Zhang, Y.; Wang, J. *J. Am. Chem. Soc.* **2014**, *136*, 3013−3015.

(5) For selected examples, see: (a) Chen, P.-H.; Sieber, J.; Senanayake, C. H.; Dong, G. *Chem. Sci.* **2015**, *6*, 5440−5445. (b) Chen, P.-H.; Xu, T.; Dong, G. *Angew. Chem., Int. Ed.* **2014**, *53*, 1674−1678. (c) Xu, T.; Ko, H. M.; Savage, N. A.; Dong, G. *J. Am. Chem. Soc.* **2012**, *134*, 20005−20008. (d) Xu, T.; Dong, G. *Angew. Chem., Int. Ed.* **2014**, *53*, 10733−10736. (e) Xu, T.; Savage, N. A.; Dong, G. *Angew. Chem., Int. Ed.* **2014**, *53*, 1891−1895. (f) Deng, L.; Xu, T.; Li, H.; Dong, G. *J. Am. Chem. Soc.* **2016**, *138*, 369−374.

(6) Juliá-Hernández, F.; Ziadi, A.; Nishimura, A.; Martin, R. *Angew. Chem., Int. Ed.* **2015**, *54*, 9537−9541.

(7) See the Supporting Information for more computational details.

(8) See Figure S2: the C1−C2 and C1−C8 cleavage mechanisms for *n*-Hex case.

(9) Lu, G.; Fang, C.; Xu, T.; Dong, G.; Liu, P. *J. Am. Chem. Soc.* **2015**, *137*, 8274−8283.

(10) The Rh(I) catalyst also plays a key role in enabling preferential C1−C8 cleavage over C1−C2 cleavage reported by Liu (Scheme S3).

(11) (a) Hong, X.; Liang, Y.; Houk, K. N. *J. Am. Chem. Soc.* **2014**, *136*, 2017−2025. (b) Ess, D. H.; Houk, K. N. *J. Am. Chem. Soc.* **2007**, *129*, 10646−10647. (c) Legault, C. Y.; Garcia, Y.; Merlic, C. A.; Houk, K. N. *J. Am. Chem. Soc.* **2007**, *129*, 12664−12665. (d) Ess, D. H.; Houk, K. N. *J. Am. Chem. Soc.* **2008**, *130*, 10187−10198. (e) Liu, F.; Liang, Y.; Houk, K. N. *J. Am. Chem. Soc.* **2014**, *136*, 11483−11493. (f) Green, A. G.; Liu, P.; Merlic, C. A.; Houk, K. N. *J. Am. Chem. Soc.* **2014**, *136*, 4575−4583.

(12) The distortion/interaction model is also called the activation-strain model: (a) van Zeist, W.-J.; Bickelhaupt, F. M. *Org. Biomol. Chem.* **2010**, *8*, 3118−3127. (b) Fernández, I.; Cossío, F. P.; Bickelhaupt, F. M. *J. Org. Chem.* **2011**, *76*, 2310−2314. (c) Fernández, I.; Bickelhaupt, F. M. *J. Comput. Chem.* **2012**, *33*, 509−516. (d) Fernández, I.; Wolters, L. P.; Bickelhaupt, F. M. J. *J. Comput. Chem.* **2014**, *35*, 2140−2145.

(13) The subsequent reductive elimination from **J** is shown in Scheme S4.

(14) In order to see if the calculated results are dependent on the method and basis set used, we did a testing calculation using another method and basis set for the key species in Table 1. See Table S1 in the Supporting Information.

(15) For similar explanation, see: Lu, Q.; Wang, B.; Yu, H.; Fu, Y. *ACS Catal.* **2015**, *5*, 4881−4889.

(16) See Figure S3: the calculated diastereoselectivity for *n*-Hex case.

DOI: 10.1021/acs.orglett.6b02943
Org. Lett. 2016, 18, 6244−6247